Rotation of terahertz radiation due to phonon-mediated magnetoelectric coupling in chiral selenium

Anirban Pal,[1] Sharmila N. Shirodkar,[2] Prathamesh Deshmukh,[1] Harshad Surdi,[1] Bagvanth R. Sangala,[1] S. S. Prabhu,[1] Kailash C. Rustagi,[1] Umesh V. Waghmare,[2] and Pushan Ayyub[1,*]

[1]*Department of Condensed Matter Physics & Materials Science, Tata Institute of Fundamental Research, Mumbai 400005, India*

[2]*Theoretical Sciences Unit, Jawaharlal Nehru Centre for Advanced Scientific Research, Bangalore 560064, India*

(Received 23 January 2018; revised manuscript received 22 September 2018; published 20 December 2018)

The trigonal form of selenium (t-Se) has an unusual, quasi-one-dimensional, *chiral* crystal structure. First-principles calculations have helped us uncover a polar, optic phonon in t-Se that exhibits a diagonal magnetoelectric coupling with the electric field of the incident THz radiation, and induces a parallel magnetic field due to its inherent chirality. We show that this phonon-mediated, magnetoelectric mechanism is predicted to cause optical rotation in t-Se in the 1–3 THz range and is quite distinct from the high frequency (>80 THz) activity due to electronic excitations that has been reported previously. In the second part of the paper, we report our experimental results based on THz time-domain spectroscopy as well as direct measurements of optical rotation that confirm this prediction in an aligned, monocrystalline array of t-Se microrods. The Se microrod array not only exhibits a large birefringence ($\Delta n = 1.3$) but also rotates the polarization of THz radiation by $\sim 3°$/mm. To our knowledge, this is the only *elemental solid* known to rotate THz polarization, because the currently available THz rotators are based mainly on liquid crystals or metamaterials. The identification of new THz-active materials and a better understanding of the underlying physics are both clearly essential to the development of better sources, detectors and components.

DOI: 10.1103/PhysRevB.98.235141

I. INTRODUCTION

Progress in the emerging field of terahertz technology [1–4], with critical applications to areas that include defense, communication, and detection of hazardous substances, depends crucially on the development of better sources, detectors, and components. However, the generation and manipulation of electromagnetic radiation in the THz window (∼0.1–10 THz) has proved to be a constant challenge. Clearly, a better understanding of the underlying physics would not only facilitate further advances in THz technology, but may also lead to the identification of new THz-active materials. Though the vibrational frequencies of solids (typically ranging from 0 to 10 THz) perfectly covers the THz window, the current generation of optical rotators in the THz region are mostly based on liquid crystals [5] or metamaterials [6]. It is important to note that it is essentially the *chirality* of certain organic molecules that leads to their vibrational optical activity, as recently established by Lombardi and Nafie [7] and Rhee *et al.* [8]. Since there exists a robust causal correlation between the structure and properties of crystalline solids, the above observation prompts us to investigate the optical (THz) activity of inorganic or metallic crystals with a *chiral structure*.

In this paper, we address the above issue for the interesting case of trigonal selenium (t-Se), whose structure consists of hexagonal arrays of helical chains parallel to the c axis, with three atoms per unit cell. The strong covalent bonding between intrachain atoms and the weak interchain interaction give rise to a *quasi-one-dimensional*, *chiral* structure that has also been recently found to be responsible for its unexpected multiferroic behavior [9]. Trigonal selenium is one of the very few elemental metals with a helical structure. That, along with the fact that its unit cell contains more than two atoms, allows t-Se to sustain infrared (IR) active phonons [10], unlike most similar elements such as cubic Si, Ge, and C. This is evident in its nonzero Born effective charges (Z*) with $|Z^*|_{\max} = 0.74|e|$, e being the electron charge (see Table I). We show in this paper, that the chiral structure allows tangential electric dipole moments on the Se helix, whose oscillation produces a magnetic field along the helical axis and leads to a magnetoelectric interaction mediated by the IR-active phonons, even in the absence of magnetic order or surface spins. Such an effect should be observable as the optical rotation of low frequency (THz) radiation, similar to that shown by chiral molecules in the mid-IR range, which is known to arise from vibrational circular birefringence [7,8]. This expectation provided us the motivation to carry out an experimental investigation of the optical properties of parallel arrays of t-Se microrods in the THz region by time-domain spectroscopy and other complementary measurements. The results of such studies provided clear experimental confirmation of the above prediction, leading to the identification of t-Se as a unique THz-active element.

II. PHONON-MEDIATED MAGNETOELECTRIC COUPLING IN TRIGONAL SELENIUM

A. Analytical Methods

Our theoretical analysis of magnetoelectric coupling was based on a first-principles approach within the density functional theory (DFT) with the generalized gradient

*Author to whom correspondence should be addressed: pushan.ayyub@gmail.com

TABLE I. Born effective charges on the three atoms in the unit cell of trigonal Se (N is the atom number and R is the direction of displacement).

		Direction of electric field		
N	*R*	*X*	*Y*	*Z*
1	*x*	0.70	0.00	0.00
1	*y*	0.00	−0.70	−0.74
1	*z*	0.00	−0.38	0.00
2	*x*	−0.35	−0.61	0.64
2	*y*	−0.61	0.35	0.37
2	*z*	0.33	0.19	0.00
3	*x*	−0.35	0.61	−0.64
3	*y*	0.61	0.35	0.37
3	*z*	−0.33	0.19	0.00

approximation (GGA) and Perdew-Burke-Ernzerhof [11] functional for exchange correlation energy as implemented in the ABINIT [12] code. An energy cutoff of 70 Ry was used in truncating the plane wave basis in representation of the Se wavefunctions. The Brillouin zone integrations were sampled over a $9 \times 9 \times 9$ mesh of **k** points. The zone center phonons and Born effective charges for a unit cell of trigonal Se were determined using DFT linear response as implemented in the ABINIT package.

B. Derivation of Magnetoelectric Coupling in Chiral Se

Symmetry analysis suggests that there are three IR-active phonons [13,14] in t-Se: a doubly degenerate E mode with $\nu_x = \nu_y = 140\,\mathrm{cm}^{-1}$, that couples with E_x and E_y, [see Figs. 1(a) and 1(b)] and an A_2 mode with $\nu_z = 102\,\mathrm{cm}^{-1}$ that couples to E_z, as shown in Fig. 1(c). Here $\boldsymbol{E}$ is the electric field of the incident radiation, **z** is along the c axis of the crystal (helicity axis), and the position vectors of the Se atoms with respect to the center of the helix are shown in Fig. 1(d). We show that the A_2 mode involves a rotation of the Se helix, which generates an oscillatory tangential displacement current and consequently an axial magnetic field (solenoid effect). Through this diagonal magnetoelectric coupling, the A_2 phonon rotates the plane of polarization of THz radiation propagating normal to z. We first derive an expression for the phonon-mediated magnetoelectric coupling (χ) in chiral media, for the specific case of t-Se.

The electric field along the z axis (E_Z) imparts a force on each Se atom along the direction tangential to the helix, $F_t = Z_t^* E_Z$, producing a tangential displacement [see Fig. 1(c)]:

$$u_{i,t} = \frac{Z_t^* E_z}{m^* \left(\omega_{A_2}^2 - \omega^2\right)}, \tag{1}$$

where $Z_t^* = 0.74|e|$, $\omega_{A2} =$ frequency of the A_2 mode ($= 2\pi\nu_z$), and $m* =$ effective mass of Se. The tangential displacements give rise to electric dipoles at each Se site with

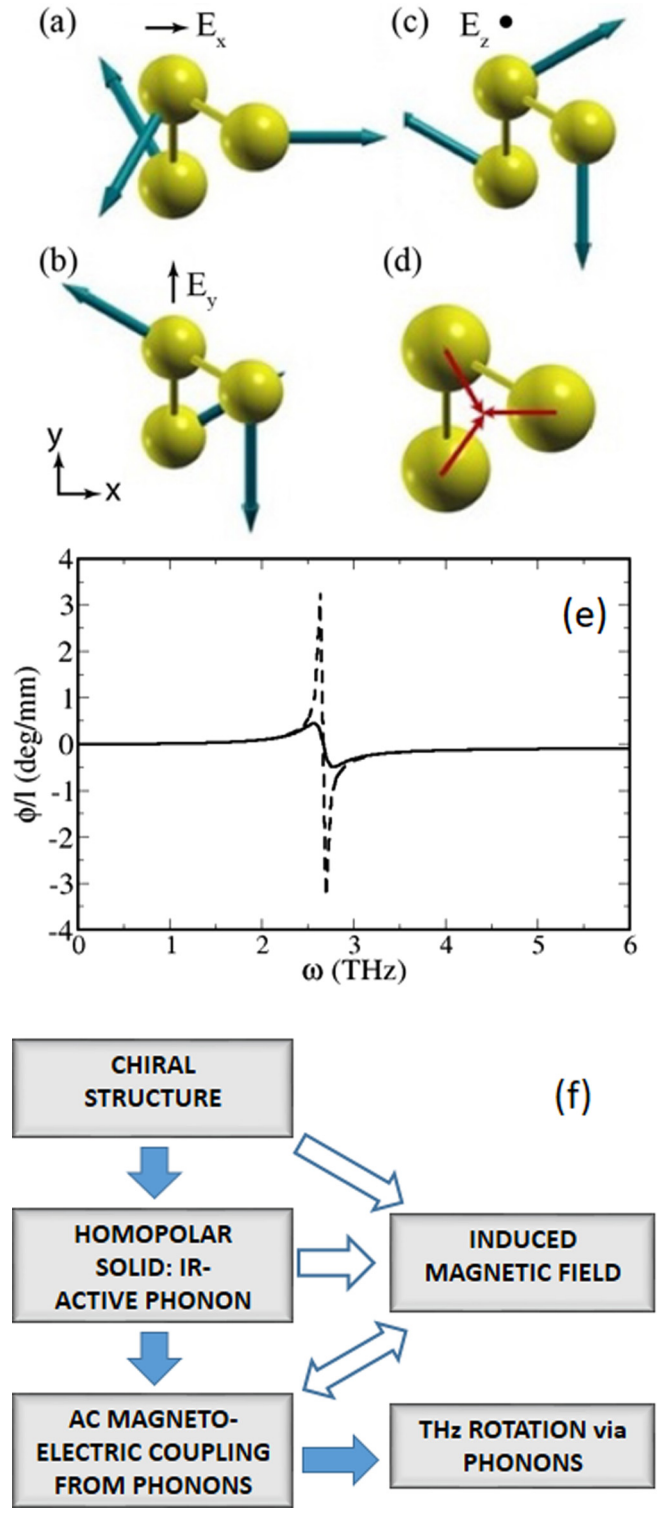

FIG. 1. Phonon modes in trigonal Se that couple with electric field applied along (a) x, (b) y, and (c) z directions. The third one involves rotation of Se helical chain about its axis. (d) The position vectors of the Se atoms with respect to the center of the helix are indicated by arrows. (e) Calculated frequency dependence of the angle of rotation per unit length, φ/l, with (solid line) and without (dashed line) correction for finite phonon line width ($\approx 7\,\mathrm{cm}^{-1}$). The electric field of the incident radiation is along the axis of the Se helix. (f) Flowchart depicting the mechanism of polarization rotation in a chiral solid such as trigonal Se.

tangential and axial components given, respectively, by

$$p_{i,t} = \frac{Z_d^* Z_t^* E_Z}{m^*\left(\omega_{A_2}^2 - \omega^2\right)} \quad \text{and} \quad p_{i,a} = \frac{Z_t^* Z_t^* E_Z}{m^*\left(\omega_{A_2}^2 - \omega^2\right)}, \quad (2)$$

where $Z_d^* = 0.70|e|$ is the diagonal in-plane Born charge (same for each Se atom). We now estimate the magnetic field induced by the time-dependent oscillation of the tangential electric dipole moments ($p_{i,t}$) by approximating each helical Se chain by a solenoid of n ($= 3/c$) turns per unit length carrying a current $I = \dot{p}_{i,t}/2\pi R$:

$$\boldsymbol{B} = \mu_o n \boldsymbol{I} = \mu_o \frac{3}{c} \frac{d\boldsymbol{p_t}/dt}{2\pi R}$$
$$= \mu_o \frac{3}{c} \frac{i\omega p_t}{2\pi R} = -i \frac{\mu_o}{4\pi} \frac{6\omega p_t}{Rc} z, \quad (3)$$

where c is the lattice constant of t-Se along the z direction, R is the radius of the Se helix, and μ_0 is the free-space permeability. Similar equations for the magnetic field components can also be obtained by treating each Se atom as a moving point charge (= the Born dynamical charge) and calculating the resulting magnetic field. Since this approach allows one to readily visualize the phonon modes that give rise to the axial magnetic field, we present it in Appendix A.

In chiral media, it is convenient to use the Tellegen form of constitutive relationships [15] for a monochromatic electromagnetic wave:

$$\boldsymbol{D} = \varepsilon \boldsymbol{E} - i\chi \boldsymbol{H} \quad \text{and} \quad \boldsymbol{B} = \mu \boldsymbol{H} + i\chi \boldsymbol{E}, \quad (4)$$

where the parameter χ represents the nontrivial chirality of the medium. Clearly, χ is identical to the magnetoelectric coupling constant and can be expressed as

$$\chi = -i \frac{\partial \boldsymbol{B}}{\partial \boldsymbol{E}} = -i \frac{\partial B_z}{\partial E_z} = -\frac{\mu}{4\pi} \frac{6\omega}{Rc} \frac{\partial p}{\partial E_z}. \quad (5)$$

The negative sign indicates that the induced magnetic field is opposite to the applied electric field. Substituting for $\boldsymbol{p}$ from Eq. (2), we get

$$\chi = -\frac{\mu}{4\pi} \frac{6\omega}{Rc} \frac{Z_d^* Z_t^*}{m^*\left(\omega_{A_2}^2 - \omega^2\right)}. \quad (6)$$

C. Estimation of Phonon-mediated THz Rotation in Chiral Se

It is clear from the above that only the A_2 phonon induces a nonzero magnetic field ($\boldsymbol{B}_z$) in t-Se, induced by the rotatory motion of the helix. $\boldsymbol{B}_z$ is normal to the incident magnetic field: $\boldsymbol{B}_{xy} = \boldsymbol{B}_x + \boldsymbol{B}_y$. The resultant magnetic field $\boldsymbol{B}_{\text{eff}} = \boldsymbol{B}_{xy} + \boldsymbol{B}_z$ clearly implies that the polarization of the magnetic field (as well as that of the electric field) *rotates* as the radiation passes through the crystal. A Se crystal of thickness l rotates the polarization of electromagnetic radiation of frequency ω by an angle [15] $\varphi = \chi\omega l$. Hence, using Eq. (6), we obtain an expression for the specific rotation:

$$\frac{\varphi}{l} = \chi\omega = \frac{\mu}{4\pi} \frac{6\omega^2}{Rc} \frac{Z_d^* Z_t^*}{m^*\left(\omega_{A_2}^2 - \omega^2 + i\gamma\omega\right)}, \quad (7)$$

where an additional (damping) term has been included in the denominator to take care of the finite lifetime of phonons. Figure 1(e) shows the calculated frequency dependence of φ/l in the low THz range, with $R = 1$ Å, $c = 4.95$ Å, $Z^* = 0.74e$, $\omega_{A2} = 102\,\text{cm}^{-1} = 3.0$ THz. For monoatomic media, the reduced mass of a phonon is just the atomic mass: [16] $m^* = 78.96 \times 1.67 \times 10^{-27}$ kg. We find that the calculated polarization rotation (φ/l): (a) peaks as $\omega \to \omega_{A2}$ with a maximum value of $\approx 3^\circ$/mm at 3.06 THz, and (b) vanishes in the low frequency ($\omega \to 0$) limit, but (c) approaches a constant value of -0.08°/mm at high frequencies ($\omega \to \infty$). Since the resonance is broadened by phonon damping (γ), the actual value of (φ/l) depends on the phonon line width, which is estimated [14] to be $7\,\text{cm}^{-1}$. We point out that the contribution of *electronic* excitations in Se at 375 THz and 88 THz causes rotations as large as 300°/mm [17] and 4.8°/mm [18], respectively, but reduces to less than $\sim 0.0006^\circ$/mm at 1 THz. However, whereas the high frequency (near-IR) response has an *electronic* origin [19], the mechanism proposed here is entirely phonon-mediated and can be traced directly to the chiral structure of the α-Se crystal. A schematic depiction of our mechanism appears in Fig. 1(f). The three-atom primitive cell has neither reflection symmetry nor inversion symmetry, which allows the existence of IR-active phonons. In particular, the atomic oscillations along the tangent to the Se helix induce a magnetic field along the helical axis. The effective phonon-mediated magnetoelectric coupling gives rise to rotation of polarization of photons in the THz frequency range.

We now describe the experimental investigation of optical rotation at low-THz frequencies in Se crystals. Our observations clearly establish the phonon-mediated mechanism of THz rotation predicted above. The main experimental challenge in detecting optical rotation in Se arises from the fact that it is also birefringent in the THz region [14].

III. EXPERIMENTAL METHODS

A. Fabrication and Characterization of Se Microrods

Single crystalline microrods of t-Se were synthesized by vapor-condensation [20,21] from amorphous Se (99.999% pure) beads heated in a quartz tube in an atmosphere of 99.99% Ar. The t-Se microrods were in the form of perfect hexagonal prisms with sharply defined facets, typically ≈5-mm long and ≈100 μm in diameter [Fig. 2(a)]. X-ray diffraction data [Fig. 2(b)] confirm the formation of the trigonal phase of Se and the absence of any other impurity phase. The measured lattice constants ($a = b = 0.4367$ nm, $c = 0.4952$ nm) were within 0.2% of the corresponding reported values (JCPDS Datafile 42–1425). Electron diffraction indicates a perfectly monocrystalline lattice [Fig. 2(c)]. The crystallographic c axis was parallel to the sixfold axis of the hexagonal prism-shaped rods. Unless otherwise mentioned, all the optical measurements were carried out on two parallel arrays of t-Se microrods that were closely stacked to make sure that no air gaps remained between them. The net thickness of such a stack was in the 150–180 μm range.

B. Measurement of Optical Properties in the THz Region by Time-Domain Spectroscopy

Optical properties of the t-Se microrods were studied in the THz region by the time-domain spectroscopy (TDS) technique, depicted schematically in Fig. 3(a). THz pulses were generated from a standard LT-GaAs commercial THz

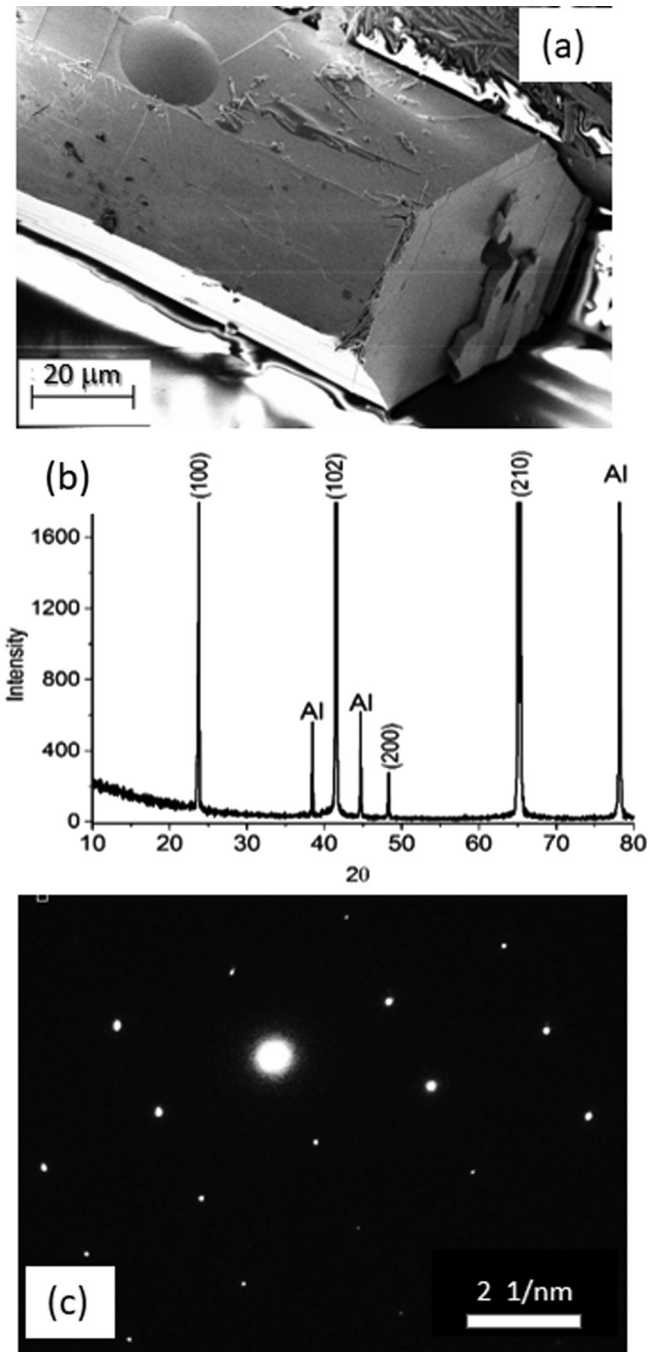

FIG. 2. (a) Scanning electron micrograph of a typical, perfectly faceted, hexagonal microrod of vapor-deposited, monocrystalline Se (diameter $\approx$ 50 μm). (b) Powder x-ray diffractogram showing the pure trigonal/hexagonal phase of Se (SG = 152 or $P3_121$). The Al lines are from the sample holder. (c) Electron diffraction pattern confirming the monocrystalline trigonal structure.

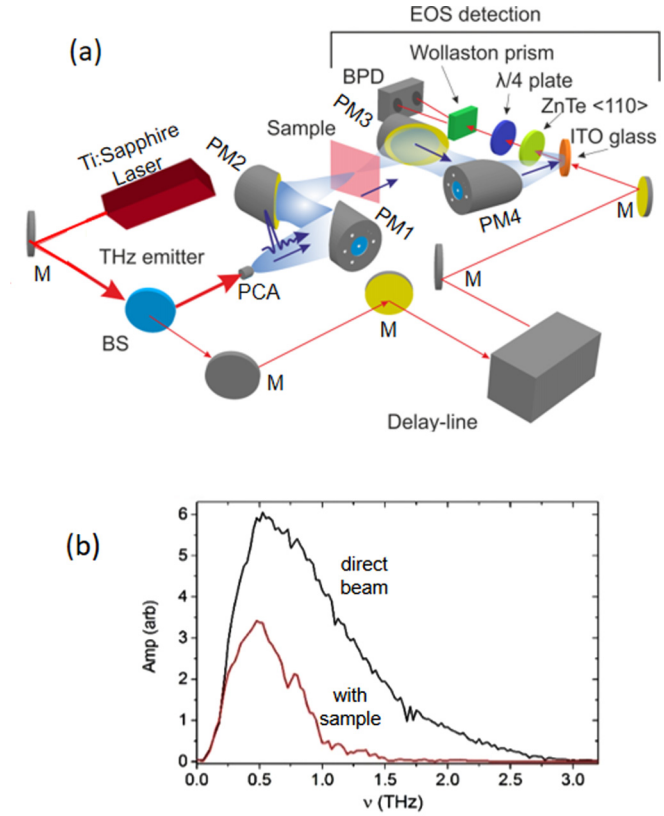

FIG. 3. (a) Schematic diagram of the time-domain spectroscopy (TDS) setup, consisting of the THz emitter, sample assembly, electro-optic detector, and associated optics. Legends: M = plane mirror, PM = parabolic mirror, BS = beam splitter, PCA = photoconducting antenna, EOS = electro − optic sampling, BPD = balanced photodiodes. (b) THz source spectra before and after passing through the microrod array sample.

photo-conducting antenna (PCA) from BATOP GmbH, gated by 800 nm, 10 fs, 76 MHz, 100 mW optical pulses from a Ti:Sapphire laser (Synergy model, Femtolasers GmbH). The laser beam was split in two parts by a beam splitter (BS), the transmitted component going to the electro-optic sampling (EOS) detector via a delay line, while the reflected component was incident on the PCA. The PCA was biased at 10 V peak-to-peak and chopped electronically at 27 KHz. The broadband, *s*-polarized THz pulses generated from the PCA had its electric field vector vertical in the laboratory frame and propagation vector normal to the microrod axis. The source spectrum is shown in Fig. 3(b), with and without the sample in place. The incident radiation, peaked at $\approx$0.5 THz and extending up to $\approx$3 THz, passed through a focusing system with four parabolic mirrors (PM1—PM4), with the sample symmetrically mounted in between PM2 and PM3. The electric field of the THz radiation incident on the electro-optic ZnTe crystal biases it, thereby elliptically polarizing the 800-nm probe beam passing through it, by an extent proportional to the strength of the THz field. The elliptically polarized probe beam was then passed through a quarter wave (λ/4) plate, which converts it to linearly polarized light. A Wollaston prism splits it into two orthogonal components, which were detected by two balanced photo-diodes (BPD) in the differential mode. By continuously changing the delay time, it is thus possible to record the entire THz pulse profile. The sample was rotated in equal steps from $\theta = 0^\circ$ to 360° using a computerized stepper motor and time domain spectra were recorded for each value of θ, the angle between the incident electric field vector and the microrod axis. The experimental setup was enclosed in a chamber purged with dry nitrogen gas to avoid THz absorption by water vapor.

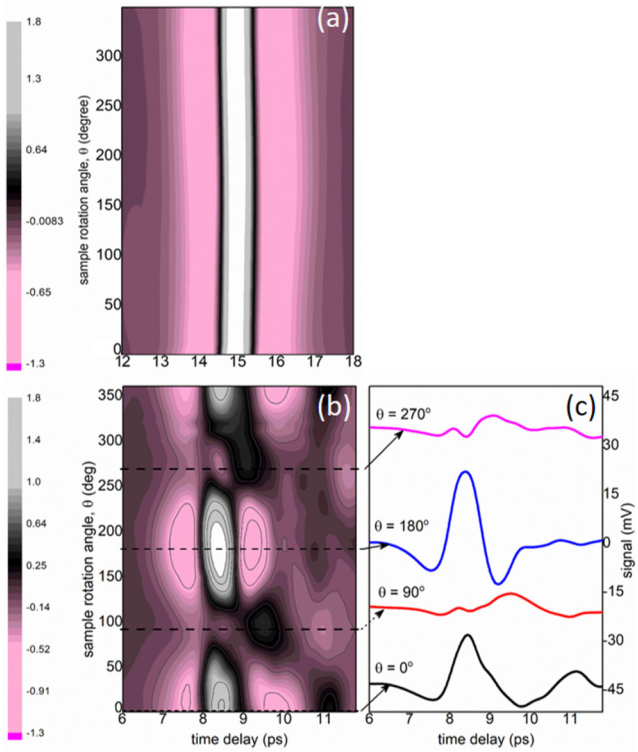

FIG. 4. THz time domain spectra, i.e., contour plots of the amplitudes of the transmitted intensity as a function of the relative time delay, recorded at all polarization angles from 0° to 360°, for (a) an amorphous Se plate, and (b) a Se micro-rod array (color scales shown beside the spectra). The corresponding line scans for the micro-rod array at a few selected angles are shown in (c).

IV. RESULTS AND DISCUSSION

A. Time-Domain Spectroscopy

The TDS spectra consist of contour plots of the *amplitudes* of the waveforms transmitted through the sample as a function of the time delay (in ps) and the sample rotation angle, θ. Such spectra were recorded for several crystalline microrod-shaped Se samples, as well as an amorphous Se plate of similar thickness, in order to distinguish between the effects of birefringence and optical rotation. The color coding used in Fig. 4 shows large positive (negative) amplitudes in shades of light grey (pink) and smaller amplitudes in shades of dark grey as depicted by the scale bars on the right. While the data for a thin amorphous Se plate shows, expectedly, no angular dependence at all [Fig. 4(a)], the monocrystalline Se microrods show a strong angular anisotropy [Fig. 4(b)]. On traversing the sample (two layers of parallel microrods) of average total thickness, $l \approx 150\ \mu$m, the incident THz beam splits into two components, polarized along and normal to the crystallographic c axis. Birefringence causes the ordinary (o) and extraordinary (e) components to travel with different velocities within the sample and arrive at the detector with a relative phase shift. Here, the stronger o component (white, with $\theta \approx 175° \pm \pi$) is detected at a delay of 8.4 ps, and the weaker e component (black, with $\theta \approx 85° \pm \pi$) at 9.5 ps. Even though the contour plots provide us with a complete picture of the amplitude profile in the θ-t space, the exact values of the peaks can be identified more accurately from the actual time spectra at the selected values of θ (corresponding to the strong and weak components) as shown in Fig. 4(c). In fact, the TDS data show the signatures of the o and e components, mutually shifted by $\pi/2$, with a high degree of precision. The fact that such an observation is possible, is a unique feature of THz-TDS, and is very difficult, if not impossible, to observe in other parts of the electromagnetic spectrum.

From the time delay measurements, we obtained: $n_o = 2.1$ and $n_e = 3.4$ for the Se microrods, while the corresponding values [14] for bulk Se are $n_o = 2.73$ and $n_e = 3.5$ and our first-principles estimates are 2.8 and 3.6, respectively. The target used in our experiments should be considered a composite of rod-shaped Se crystals with narrow cylindrical holes parallel to the z axis, for which the effective dielectric constant $\langle \varepsilon_{zz} \rangle$ is the weighted average of ε(Se) and ε(air) [22]. However, it is possible for $\langle \varepsilon_{xx} \rangle$ to be lower than the corresponding weighted average for positive uniaxial crystals such as Se. The measured value of the birefringence, $\Delta n \approx 1.3$, is quite high though the precision is limited to a certain extent by the noise in the TDS data.

The second important feature of the parallel microrod array target is that it acts as an efficient wire-grid polarizer for THz radiation, with an estimated extinction coefficient: $K = [E_x(\max)/E_z(\max)]^2 = (3.28)^2 = 10.74$. The best commercial wire grid polarizers have $K > 10^2$, but the Se microrods should show much better response for radiation peaked closer to 3 THz. On the other hand, a measurement of the optical constants, (n_o, n_e) in the frequency range 0.2–1.0 THz (not shown here) indicates that there is no significant free-carrier absorption in this range, which would otherwise have masked this effect.

B. Direct Measurement of Optical Rotation

Though the TDS measurements provide important information about the nature of dispersion and the optical constants of the material, it does not allow us to separate the effects of birefringence and optical rotation. The optical rotation produced by the parallel microrod array was measured directly using a bolometer and lock-in amplifier setup shown in Fig. 5(a). Initially, without the sample being present, the analyzer was oriented in a crossed position (minimum transmitted intensity) with respect to the vertically polarized incident THz radiation. The sample was then mounted on a rotatable holder and the intensity recorded as a function of the sample rotation angle θ. The experimental geometry is shown in Fig. 5(b). The total contribution from birefringence and optical rotation was estimated by fitting the angular dependence of the transmitted intensity [Fig. 6(a)] to the equation [23]

$$I \sim (\alpha k^2)^2 \left[\frac{(\sin\theta)^2}{k n_e} - \frac{(\cos\theta)^2}{k n_o} \right]^2 + (k n_e - k n_o)^2 (\sin 2\theta)^2, \tag{8}$$

which has been derived in Appendix B. Here α is the off-diagonal term of the dielectric tensor. Fitting Eq. (8) to the experimental data ($n_o = 2.1$, $n_e = 3.4$), we obtain $\alpha = 7.0$. The corresponding value of specific rotation for Se microrods is much higher than the theoretical estimate. This is probably due to the microrods not being perfectly parallel, which would

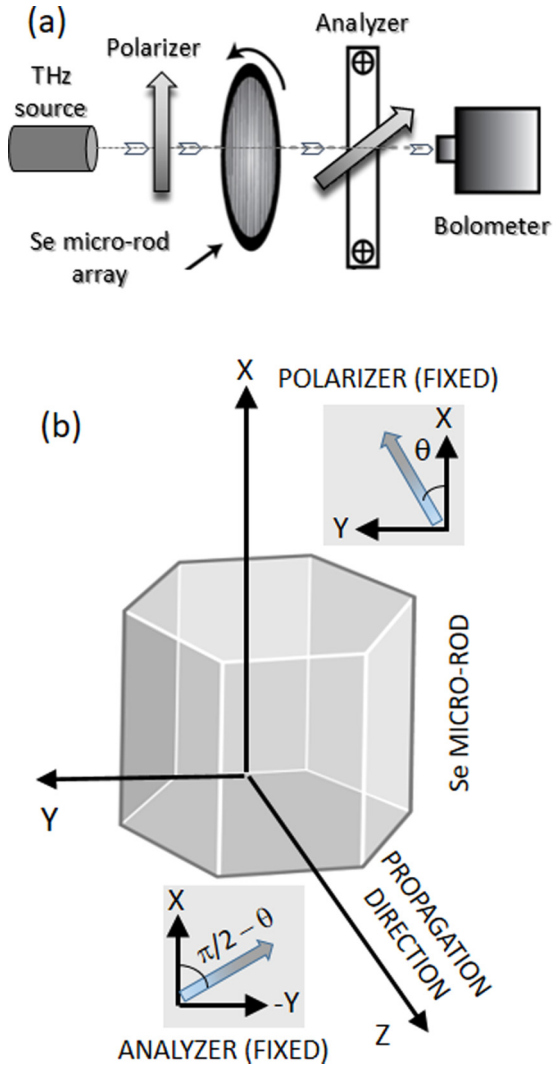

FIG. 5. (a) Experimental setup for measuring the optical rotation due to Se microrod array (sample rotated) or polycrystalline Se (analyzer rotated). (b) The experimental geometry pertaining to this problem, showing the orientations of the Se microcrystal axes with respect to the polarization vectors of the THz radiation at the point of incidence into the Se microrod and just after emerging from it.

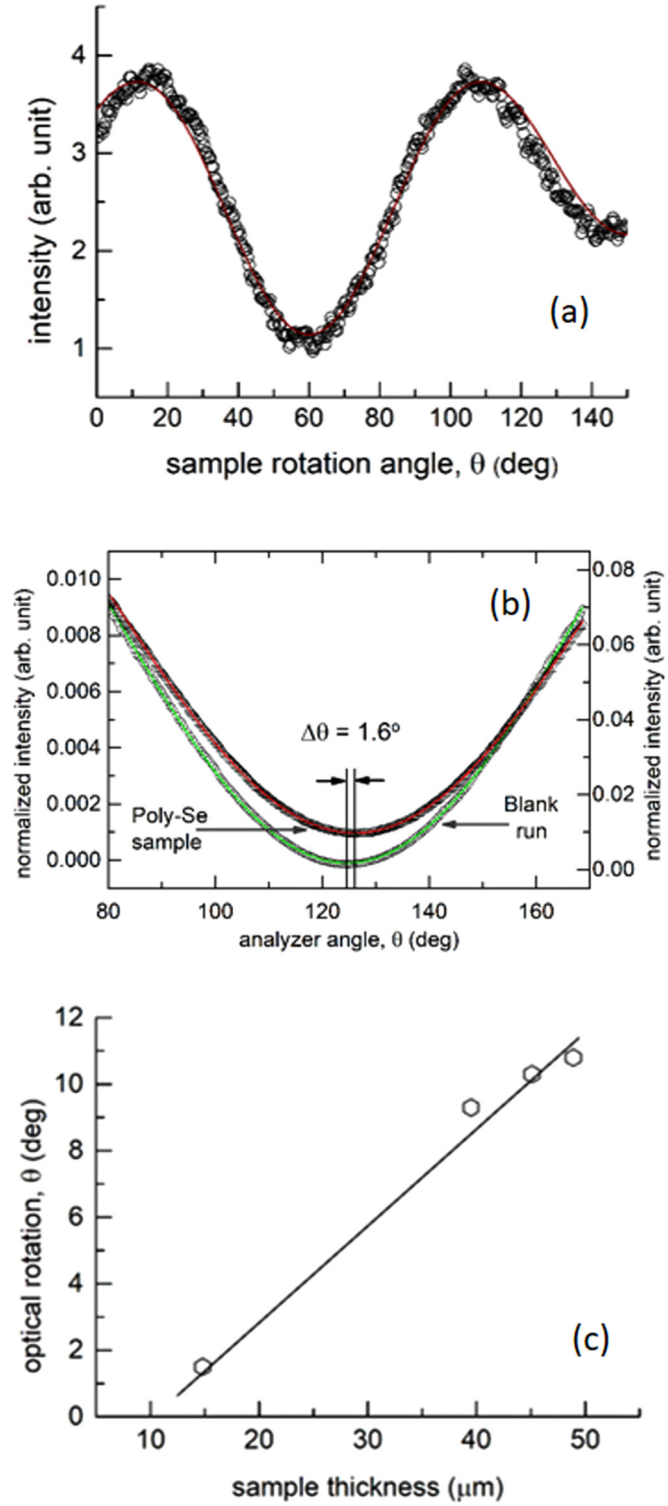

FIG. 6. (a) Angular dependence of the intensity transmitted through the microrod array. (b) Angular shift showing the polarization rotation produced by a polycrystalline Se sample. (c) Thickness dependence of the THz rotation produced by polycrystalline Se.

lead to some degree of coupling between the two polarizations arising from birefringence. Our data clearly indicates the interesting possibility of *tailoring the birefringence* by appropriately stacking or orienting the microrods and thereby controlling the coupling between the microrods. This provides the opportunity of designing useful polarization-based devices such as iso-index filters [24–26].

The optical rotation was also measured in polycrystalline pellets of Se, in which the birefringence is expected to be strictly zero, due to the absence of a unique optic axis. We used the same setup as above [Fig. 5(a)], but recorded the transmitted intensity as a function of the rotation angle of the *analyzer*, while keeping the sample and incident polarization fixed. In the absence of the sample, the minimum intensity recorded at the detector corresponds to the crossed polarizer/analyzer position. The shift in the angle of minimum intensity ($\Delta\theta$) due to introduction of the Se sample directly gives the optical rotation, as seen in Fig. 6(b). The measured values of $\Delta\theta$ in Se samples of different thickness are plotted in Fig. 6(c), from which we obtain the specific optical rotation as 2.8°/mm, in very good agreement with our theoretical

prediction of 3°/mm. Note also that the experimental result represents an "integrated" value over a range of frequencies, while the prediction refers to the *peak* value at resonance.

In summary, we have proposed a mechanism for polarization rotation of low-THz radiation arising from phonon-mediated magnetoelectric coupling in chiral crystals such as trigonal Se. In this crystal, an IR-active phonon couples to the electric field along the helical axis of the crystal and produces an axial ac-magnetic field. It is also important to point out that the magnetoelectric coupling arises purely from the chiral structure of Se, and does not involve surface spins. Our experiments confirm that monocrystalline t-Se microrods act as polarization rotators, as well as efficient wire-grid polarizers. The resonant phonon-mediated THz activity in Se should be significantly higher for a beam profile peaked around 3 THz. Our results strongly suggest that the chiral phase of Se microrods holds significant promise as a future THz-active material, as it has also been recently shown to be an excellent THz emitter [4]. Our discovery of THz activity in a simple chiral inorganic semiconductor should stimulate the search for other materials with applications to terahertz technology.

ACKNOWLEDGMENTS

S.N.S. thanks the Council of Scientific and Industrial Research, Government of India, for a Research Fellowship. U.V.W. acknowledges support from a JC Bose National Fellowship of the DST, Government of India, and a RAK CAM Sheikh Saqr Fellowship.

APPENDIX A: CALCULATION OF MAGNETOELECTRIC COUPLING IN TRIGONAL Se

The magnetic field within a Se helix was calculated in Sec. II B using Ampere's law, treating the helix as a solenoid. The magnetic field components due to the external electric field on the Se atoms are derived here by treating each Se atom as a moving point charge equal to the Born dynamical charge, and finally using the formula for the magnetic field of a moving point charge. This approach also provides information on the particular phonon modes that are responsible for the axial magnetic field. The magnetic field at the axis of the helical Se chain induced by the motion of the i^{th} atom, considered as a point charge q with velocity v_i, position vector r_i (in the azimuthal plane), electric dipole moment p_i and frequency of oscillation ω, is

$$B = \sum_i B_i = \sum_i \frac{\mu_o}{4\pi}\frac{q[v_i \times r_i]}{r_i^3} = \sum_i \frac{\mu_o}{4\pi}\frac{[\dot{p}_i \times r_i]}{r_i^3} = \sum_i \frac{\mu_o}{4\pi}\frac{[i\omega p_i \times r_i]}{r_i^3}. \quad \text{(A1)}$$

For simplicity, we consider the effects of the electric field in the x, y, and z directions independently and estimate the magnetic field ($\boldsymbol{B}$) induced at the center of a helical chain of Se atoms.

Case I: $E_x \neq 0$ and $E_y = E_z = 0$ ($\theta = 90°$, $\varphi = 0°$):

$$\boldsymbol{B}_1 = \frac{\mu_o}{4\pi}\frac{[i\omega \boldsymbol{p}_1 \times \boldsymbol{r}_1]}{r_1^3} = 0,$$

$$\boldsymbol{B}_2 = \frac{\mu_o}{4\pi}\frac{[i\omega \boldsymbol{p}_2 \times \boldsymbol{r}_2]}{r_2^3} = \frac{\mu_o}{4\pi}\frac{i\omega\sqrt{3}p/2}{R^2}z,$$

$$\boldsymbol{B}_3 = \frac{\mu_o}{4\pi}\frac{[i\omega \boldsymbol{p}_3 \times \boldsymbol{r}_3]}{r_3^3} = -\frac{\mu_o}{4\pi}\frac{i\omega\sqrt{3}p/2}{R^2}z.$$

$$\text{Hence: } \boldsymbol{B} = \boldsymbol{B}_1 + \boldsymbol{B}_2 + \boldsymbol{B}_3 = 0. \quad \text{(A2)}$$

Case II: $E_y \neq 0$ and $E_x = E_z = 0$ ($\theta = 90°$, $\varphi = 90°$), we can similarly show

$$\boldsymbol{B}_1 = 0,$$

$$\boldsymbol{B}_2 = -\boldsymbol{B}_3 = \frac{\mu_0}{4\pi}\frac{i\omega\sqrt{3}p/2}{R^2}z.$$

$$\text{Hence: } \boldsymbol{B} = \boldsymbol{B}_1 + \boldsymbol{B}_2 + \boldsymbol{B}_3 = 0. \quad \text{(A3)}$$

Case III: $E_z \neq 0$ and $E_x = E_y = 0$ (i.e., $\theta = 0°$, $\varphi = 0°$), we can similarly show

$$\boldsymbol{B}_1 = \boldsymbol{B}_2 = \boldsymbol{B}_3 = -\frac{\mu_o}{4\pi}\frac{i\omega p}{R^2}z,$$

$$\text{Hence: } \boldsymbol{B} = \boldsymbol{B}_1 + \boldsymbol{B}_2 + \boldsymbol{B}_3 = -i\frac{\mu_0}{4\pi}\frac{3\omega p}{R^2}z. \quad \text{(A4)}$$

The total magnetic field inside the Se helix in the bulk crystal is the sum over all the Se atoms, which finally leads to the earlier expression derived for the solenoidal magnetic field [Eq. (3)]. The conclusion that the magnetic field vanishes due to cancellation of fields on several different Se atoms [as shown here in Eqs. (A2) and (A3)] is a consequence of symmetry and remains robust even in the infinite crystal limit.

APPENDIX B: CALCULATION OF OPTICAL ROTATION FROM ANGULAR DEPENDENCE OF TRANSMITTED INTENSITY

Here we derive a general formula for the θ dependence of the intensity of the transmitted THz radiation through the t-Se sample. The experimental geometry is defined in Fig. 5(b) above. At the point of incidence ($z = 0$), the electric field of the THz radiation is, in general

$$E_{in}(0, t) = E_0(\cos\theta, \sin\theta, 0) = (E_x, E_y, 0).$$

After traveling a distance z inside the crystal, the two components of the electric field are

$$E_x(z) = \exp[-(k_x + k_y)z/2]\left[E_{0x}\cos(\delta z/2) + \frac{i\sin(\delta z/2)}{\delta}\left(E_{0x}\Delta k - \frac{k^2}{k_x}\varepsilon_{xy}E_{0y}\right)\right], \quad \text{(B1)}$$

$$E_y(z) = \exp[-(k_x + k_y)z/2]\left[E_{0y}\cos(\delta z/2) + \frac{i\sin(\delta z/2)}{\delta}\left(E_{0y}\Delta k - \frac{k^2}{k_y}\varepsilon_{yx}E_{0x}\right)\right]. \tag{B2}$$

Here $k_x = k\sqrt{\varepsilon_{xx}} = n_e\frac{\omega}{c}$ refers to the extraordinary (e) wave, and $k_y = k\sqrt{\varepsilon_{yy}} = n_o\frac{\omega}{c}$ refers to the ordinary (o) wave. If the optic axis in Se is defined as the x axis, then the refractive indices along the x and y axis are n_e and n_o, respectively. We note that the polarizer (placed before the sample) and analyzer (placed after the sample) are exactly 90° rotated with respect to each other, as shown in Fig. 5(b). The projections of the components of E_o on the analyzer axis are $E_x\cos(\frac{\pi}{2} - \theta) = E_x\sin(\theta)$ and $-E_y\cos(\theta)$.

Substituting these values in Eqs. (B1) and (B2), and simplifying, we obtain

$$E_x(z)\sin\theta = \exp[-(k_x + k_y)z/2]\left[\frac{1}{2}E_0\sin 2\theta\cos\left(\frac{\delta z}{2}\right) + \frac{k^2}{k_x\delta}\alpha E_0(\sin\theta)^2\sin\left(\frac{\delta z}{2}\right) + \frac{i\Delta k\ \sin(\delta z/2)}{2\delta}(E_0\sin 2\theta)\right], \tag{B3}$$

$$E_y(z)\cos\theta = \exp[-(k_x + k_y)z/2]\left[\frac{1}{2}E_0\sin 2\theta\cos\left(\frac{\delta z}{2}\right) + \frac{k^2}{k_x\delta}\alpha E_0(\sin\theta)^2\sin\left(\frac{\delta z}{2}\right) - \frac{i\Delta k\ \sin(\delta z/2)}{2\delta}(E_0\sin 2\theta)\right]. \tag{B4}$$

Here $\varepsilon_{xy} = -\varepsilon_{yx} = i\alpha$. The intensity of the light falling on the detector is proportional to $I \sim |E_x(z)\sin\theta - E_y(z)\cos\theta|^2$, which we can now evaluate by using Eqs. (B3), (B4) and simplifying

$$I \sim \left(\frac{\alpha k^2}{\delta}E_0\sin\left(\frac{\delta z}{2}\right)\right)^2\left[\frac{(\sin\theta)^2}{k_x} - \frac{(\cos\theta)^2}{k_y}\right]^2 + \left[\frac{\Delta k\ \sin(\delta z/2)}{\delta}E_0\right]^2(\sin 2\theta)^2.$$

Further, using $k_x = k\sqrt{\varepsilon_{xx}} = kn_e$ and $k_y = k\sqrt{\varepsilon_{yy}} = kn_o$ we get

$$I \sim (\alpha k^2)^2\left[\frac{(\sin\theta)^2}{kn_e} - \frac{(\cos\theta)^2}{kn_o}\right]^2 + (kn_e - kn_o)^2(\sin 2\theta)^2. \tag{B5}$$

The above formula provides a very good fit to the experimental data shown in Fig. 6(a). Though we have assumed negligible absorption while deriving it, the formula is clearly able to generate the main features of the observed data.

[1] A. Rostami, H. Rasooli, and H. Baghban, *Terahertz Technology: Fundamentals and Applications* (Springer, Berlin, 2011).
[2] M. Tonouchi, Nat. Photon. **1**, 97 (2007).
[3] B. Ferguson and X.-C. Zhang, Nat. Mater. **1**, 26 (2002).
[4] M. Shalaby and C. P. Hauri, Sci. Rep. **5**, 8059 (2015).
[5] H.-Y. Wu, C.-F. Hsieh, T.-T. Tang, R.-P. Pan, and C.-L. Pan, IEEE Photon. Technol. Lett. **18**, 1488 (2006).
[6] L. Cong, W. Cao, X. Zhang, Z. Tian, J. Gu, R. Singh, J. Han, and W. Zhang, Appl. Phys. Lett. **103**, 171107 (2013).
[7] R. A. Lombardi and L. A. Nafie, Chirality **21**, E277 (2009).
[8] H. Rhee, Y.-G. June, J.-S. Lee, K.-K. Lee, J.-H. Ha, Z. H. Kim, S.-J. Jeon, and M. Cho, Nature (London) **458**, 310 (2009).
[9] A. Pal, S. N. Shirodkar, S. Gohil, S. Ghosh, U. V. Waghmare, and P. Ayyub, Sci. Rep. **3**, 2051 (2013).
[10] I. Chen and R. Zallen, Phys. Rev. **173**, 833 (1968).
[11] J. P. Perdew, K. Burke, and M. Ernzerhof, Phys. Rev. Lett. **77**, 3865 (1996).
[12] X. Gonze *et al.*, Comput. Mater. Sci. **25**, 478 (2002).
[13] R. Geick, U. Schröder, and J. Stuke, Phys. Status Solidi B **24**, 99 (1967).
[14] E. J. Danielewicz and P. D. Coleman, Appl. Opt. **13**, 1164 (1974).
[15] S. J. Orfanidis, Electromagnetic Waves and Antennas. 2008 (Online: www.ece.rutgers.edu/~orfanidi/ewa).
[16] T. Nishimatsu, U. V. Waghmare, Y. Kawazoe, and D. Vanderbilt, Phys. Rev. B **78**, 104104 (2008).
[17] J. E. Adams and W. Haas, in *The Physics of Selenium and Tellurium*, edited by W. C. Cooper (Pergamon Press, Oxford, 1969), pp. 293–297.
[18] G. W. Day, Appl. Phys. Lett. **18**, 347 (1971).
[19] H. Zhong, Z. H. Levine, D. C. Allan, and J. W. Wilkins, Phys. Rev. Lett. **69**, 379 (1992).
[20] L. Ren, H. Z. Zhang, P. H. Tan, Y. F. Chen, Z. S. Zhang, Y. Q. Chang, J. Xu, F. H. Yang, and D. P. Yu, J. Phys. Chem. B **108**, 4627 (2004).
[21] A. Pal, S. Gohil, S. Sengupta, H. K. Poswal, S. M. Sharma, S. Ghosh, and P. Ayyub, J. Phys.: Condens. Matter **27**, 415404 (2015).
[22] F. J. García-Vidal, J. M. Pitarke, and J. B. Pendry, Phys. Rev. Lett. **78**, 4289 (1997).
[23] M. May, S. Debrus, J. Amzallag, X. M. Hui, and A. Chevy, J. Opt. Soc. Am. A **9**, 1412 (1992).
[24] N. I. Zheludev, E. Plum, and V. A. Fedotov, Appl. Phys. Lett. **99**, 171915 (2011).
[25] P. A. Yeh, Iso-index birefringent filters. U.S. Patent No. 4500178, 19 Feb. 1985.
[26] J. P. Laurenti, K. C. Rustagi, and M. Rouzeyre, Appl. Phys. Lett. **28**, 212 (1976).